The International Journal of Advanced Manufacturing Technology (2018) 99:1825–1837
https://doi.org/10.1007/s00170-018-2515-7

ORIGINAL ARTICLE

On the design and application of hybrid electrical discharge and arc machining process for enhancing drilling performance in Inconel 718

Afzaal Ahmed[1] · M. Tanjilul[1] · A. Fardin[1] · Y. S. Wong[1] · M. Rahman[1] · A. Senthil Kumar[1]

Received: 29 November 2017 / Accepted: 25 July 2018 / Published online: 28 August 2018

Abstract
In recent years, Inconel 718 is widely used in industries like aerospace, oil and gas, and automobile due to their unique combination of hardness, strength, temperature, and corrosion resistance properties. However, these materials pose challenges during conventional machining due to their high work hardening tendency, poor thermal conductivity, and chemical affinity towards the tool material. Consequently, rapid tool wear during the machining of Inconel 718 results in poor productivity. To overcome these issues, a non-contact hybrid electrical discharge and arc machining (HEDAM) process has been developed to machine such difficult-to-cut materials. Firstly, the design and development of the HEDAM circuit has been discussed. Subsequently, the working principle of the newly developed process has been studied followed by its performance comparison with the conventional EDM process. In addition, the material removal mechanism has also been discussed in detail. Finally, experimental results were reported, where holes were drilled using the developed HEDAM process. The HEDAM process has exhibited significant improvements in terms of material removal rate (MRR) which is around 12 times higher and electrode wear ratio (EWR) that is half when compared to conventional EDM. This high performance HEDAM process resulted in successful and efficient drilling of Inconel 718.

Keywords EDM · Hybrid machining · Drilling · Inconel 718 · Material removal rate (MRR) · Electrode wear ratio (EWR)

1 Introduction

The advent of advanced engineering superalloys, like Inconel 718, have presented unprecedented challenges in the frontier of today's manufacturing industry. The challenge stems from the superior mechanical, chemical, thermal, and physical properties of the material, which makes it difficult-to-machine. In recent years, the machining of Inconel 718 has become an active area of research to meet the increasing demands of these advanced materials and to address the problems associated with their machinability. The factors which makes the machining of Inconel 718 challenging to the manufacturing industry are the following: (1) a major portion of its strength is maintained during machining due to its high temperature resilience; (2) work hardening—after the first cut, the next material layer becomes harder, leading to excessive tool wear; (3) occurrence of chemical reaction at high machining temperatures causing diffusion wear; (4) abrasion wear of cutting tools due to the presence of abrasive particles in the microstructure; (5) poor thermal conductivity of the alloy—often resulting in elevated temperatures at the tool tip exacerbating the tool wear [1–6]. The synergy of these issues restrict the processing of this material through conventional methods; thus, making them inappropriate and uneconomical to adopt. Therefore, the machinability of such difficult-to-cut materials is an important concern which calls for novel processing methods.

Electrical discharge machining (EDM) is one of the non-conventional and cost-effective methods for machining difficult-to-cut materials, regardless of their extreme mechanical properties. In EDM, the heat generated by the sparks results in the removal of material by melting and vaporization. Therefore, no mechanical cutting force exists between the workpiece and tool electrode, which liberates it from all the issues associated with conventional machining. As a result, it has become popular in various manufacturing applications. In general, EDM is able to machine products with good accuracy

✉ Afzaal Ahmed
mpeafa@nus.edu.sg; afzaalahmed86@gmail.com

[1] Present address: EA-02-17, 9 Engineering Drive 1, Department of Mechanical Engineering, National University of Singapore, Singapore 117576, Singapore

and surface finish. However, the limitation is that the machining time of EDM is high compared to other machining processes [7]. Many studies have been conducted to examine the effect of process parameters on the performance of EDM in terms of material removal rate (MRR), electrode wear ratio (EWR), surface integrity, etc. [8]. By selecting a low current and low pulse-on time, a good surface finish can be achieved [9]. However, this selection is undesirable as it makes the process prolonged with an extremely low MRR. Despite volumes of research, not much attempts have been made to investigate the application of EDM in large format machining processes where the machining time is a crucial factor. The low MRR of EDM hinders its application in such time-sensitive machining cases. Recently, Zhao et al. [10] proposed a faster non-contact method of material removal suitable for format scale machining called blast erosion arc machining (BEAM). Unlike the sparking phenomenon seen in EDM, BEAM uses a strong hydrodynamic force of high velocity flushing to break the plasma channel. When the plasma channel is broken, a shockwave is created and it removes molten material in an explosive manner. Owing its high rate of material removal, BEAM is able to machine surfaces and slots effectively. However, its application in drilling remains unexplored. This opens up opportunities to explore research in high-speed non-contact drilling.

In order to overcome the challenges during the machining of such difficult-to-cut materials, this paper present a high-speed, non-contact machining process named hybrid electrical discharge and arc machining (HEDAM). In this process, an additional DC power supply is used in conjunction with the normal EDM pulsed power supply to enhance material erosion, thereby reducing the machining time. The detailed design and development of this hybrid process have been discussed in the paper, including the reports of several drilling experiments that have been carried out to fabricate holes in Inconel 718 using the developed process. Different machining parameters like peak current, flushing pressure, and rotational speed of the electrode were evaluated to identify the main factors influencing the effectiveness of HEDAM. Furthermore, microstructure, microhardness, and surface roughness were analyzed to further investigate the applicability of HEDAM process in commercial applications.

2 Design and development of HEDAM circuit

The schematic diagram of the HEDAM circuit and the various components required for its construction is depicted in Fig. 1. Two ultra-fast recovery diodes (recovery time 200 ns) were utilized to connect the pulsed and the DC power supplies. The major objective of the developed circuit is to ensure that there will not be any cross flow of current, which can damage both the pulsed and DC power supplies. It is evident from the figure that the anode of diode 1 will draw current from DC power supply, while the anode of diode 2 will siphon current from the pulsed power supply. In order to merge one common output current from the four cathode points separated across the circuit, a copper connector plate was used.

During the HEDAM process, the diodes have to carry high magnitudes of current through them. Additionally, thicker wires of 70 mm^2 were used to accommodate high current. The crimp connectors used to connect these wires in place on the circuit had to be custom made, because the commercially available crimp connectors for holding such thicker wires are too big. Moreover, any potential short circuit was prevented by fabricating the head of the crimp connector small, so that they do not come into contact with the copper plate.

Furthermore, high current flow means large amount of heat generated. If the diodes are not adequately cooled, the diodes will get over-heated causing permanent damage. Therefore, these diodes were mounted on top of a heat sink allowing the heat to dissipate away quickly. Additionally, a white thermal epoxy (heat sink compound) was used to fill any remaining gaps between the diodes and the heat sink to maximize the thermal conductivity.

3 Working principle of HEDAM process

HEDAM can be operated in three modes. The first mode takes place when the voltage across the DC supply is lower than the voltage across the pulsed power supply. The second mode occurs when both the DC and pulsed power supply are operating at the same voltage settings. In the third case, the voltage across the DC power supply is higher than that of pulsed power supply.

3.1 Mode 1: $V_{DC} < V_{PDC}$

The working principle of HEDAM for this mode is explained with Fig. 2.

Prior to the current input from the DC power supply, the process is exactly the same as EDM, where material removal takes place only during the t_{on} time. However, when the DC power supply is turned on, current is supplied to the electrode-workpiece system during the t_{off} time, causing machining to occur during the t_{off} time as well.

As can be understood from Fig. 2a, during the t_{on} duration, the voltage across the DC power supply is lower compared to the pulse power supply. As a result, diode D2 will become forward biased while the diode D1 will be in reverse bias condition. In this situation, the current is drawn from the pulsed power supply alone. However, during t_{off} time, the voltage across the diode D2 becomes 0 ($V_{PDC} = 0$), which

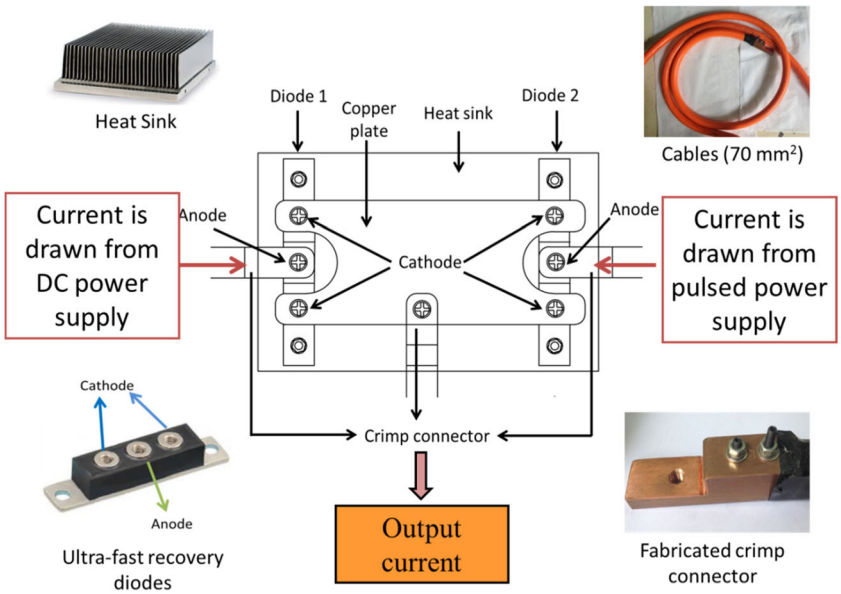

Fig. 1 Schematic diagram and components required for the fabrication

makes diode D1 forward biased and D2 reverse. Therefore, the system draws current only from the DC power supply.

Initially, when the pulse power supply is switched on, the servo CNC controller lowers itself automatically such that the electrode moves closer to the workpiece. The electric field gains the highest strength when the electrode and the workpiece are closest to each other. When the resistivity of the dielectric fluid is lowest, a single spark is generated followed by the formation of a plasma channel. In the case of EDM, during the t_{off} time, current is no longer supplied to the electrode-workpiece system and the plasma channel collapses. However, for HEDAM, the system is able to draw current from the DC power supply to maintain the plasma channel even during the t_{off} time. Due to the high pressure flushing and rotation of the tool electrode, the plasma channel eventually deionizes, causing the cycle to begin anew.

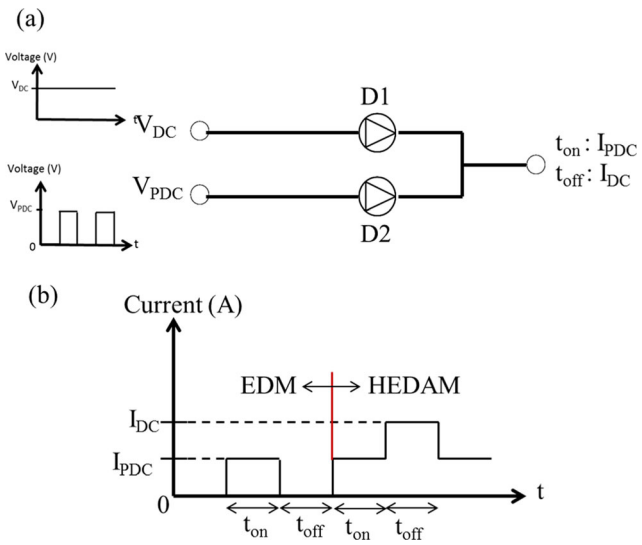

Fig. 2 Working principle of HEDAM when $V_{DC} < V_{PDC}$

3.2 Mode 2: $V_{DC} = V_{PDC}$

In this mode, during the t_{on} time of pulsed power supply, since the voltage across both the diodes is the same, both diodes D1 and D2 will be in forward bias condition and current will be drawn from both the power supplies. Therefore, the current supplied to the system is the summation from both power supplies during t_{on} time. However, during the t_{off} time of the pulsed power supply, no current will be supplied from the pulse power supply. Thus, the system will draw current from the DC power supply alone. Ideally, this mode is difficult to achieve, because the two voltages cannot be maintained at the same magnitude due to the voltage drop across the diodes. The schematic representing the circuit and current outputs is shown in Fig. 3.

3.3 Mode 3: $V_{DC} > V_{PDC}$

In this mode, the voltage across the diode D1 is higher than the diode D2, which makes the diode D1 forward biased. Thus, the system only draws current from the DC power supply, regardless of t_{on} and t_{off}, resulting in continuous arcing. This makes the pulsed power supply redundant. Moreover, the arcing leads to violent and non-uniform melting of the workpiece, which makes this mode undesirable for machining. Furthermore, the amount of debris formed in this mode maybe too much for the flushing system to handle.

In summary, during HEDAM, EDM acts as a catalyst which facilitates the formation of the initial plasma channel due to the sparking phenomena. Following the spark, the conductivity of the plasma channel decreases; but it is still sufficient enough for arc to sustain. However, due to high pressure flushing and rotation of the tool electrode, the plasma channel

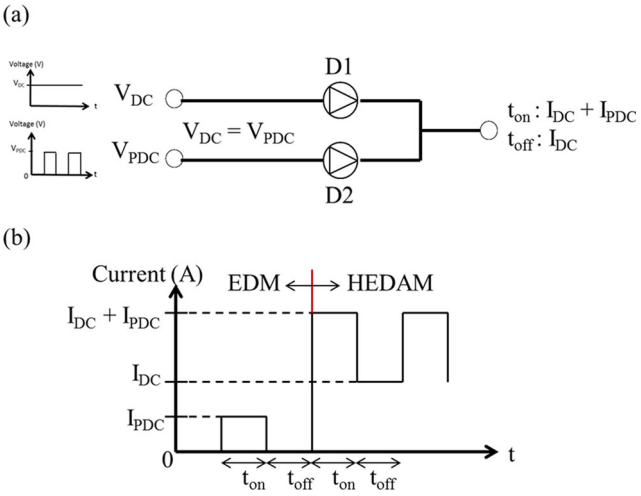

Fig. 3 Working principle of HEDAM when $V_{DC} = V_{PDC}$

eventually collapses and the ionization dies down, causing the cycle to begin again.

4 Experimental setup

The developed HEDAM high-speed drilling system is integrated into an EDM machine. In addition to the existing standard pulse generator, a DC power supply is added to facilitate HEDAM. Both the pulse generator and DC power are connected together using the developed circuit to provide a common output. The machine has a work table size of 250 mm × 350 mm and an axis travel capability of (X, Y, Z)—200 mm × 300 mm × 300 mm. In these experiments, copper-tungsten (CuW) pipe electrodes with 3.0 mm outer diameter, 0.8 mm inner diameter and 175 mm length were used. Moreover, the machine has an electrode-guiding arrangement to minimize electrode wobbling during operation. Figure 4 presents a schematic diagram of the developed experimental setup.

4.1 Machining conditions and parameters

A series of drilling experiments were conducted using mode 1 of HEDAM working principle as discussed in Section 3. Different machining conditions were applied to study the effect of the major operating parameters. The machining conditions for this study are listed in Table 1.

4.2 Comparative study of EDM and HEDAM

MRR is the volume of material removed per unit time, while EWR is a measure of the percentage of volumetric electrode wear with respect to the volume of material removed from the workpiece. It can be observed from Fig. 5 that the MRR and EWR for HEDAM drilling of Inconel 718 has shown significant improvements over conventional EDM. The MRR of HEDAM drilling (50 A from DC) is 200 mm^3/min, which is 12 times higher than that of conventional EDM drilling at 2000 rpm electrode rotational speed. On the other hand, EWR for the hybrid process is approximately 3.5%, which is much lower compared to that of EDM. Increasing the pulse current from the DC power source at a constant frequency increases the energy of the pulse leading to more melting which ultimately results in higher MRR.

Moreover, in order to investigate the effect of drilling depth on MRR and EWR, a series of experiments were conducted with varying thicknesses of workpiece. Figure 5 represents the variation of MRR and EWR for EDM and HEDAM in different thicknesses of Inconel 718 workpieces. The selected

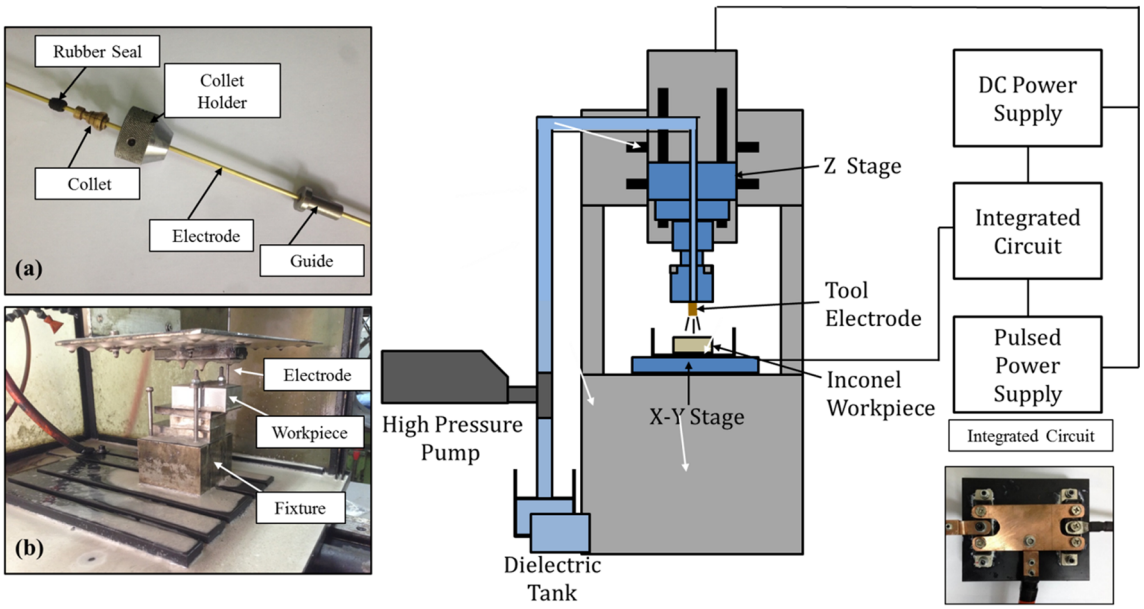

Fig. 4 Experimental setup for HEDAM **a** collet-electrode-guide arrangement and **b** electrode-workpiece arrangement

Table 1 Machining conditions for the experiments

Parameters	Machining conditions	Units
Current from the DC power supply (I_{DC})	50, 80, 110, and 140	A
Current from the pulsed power supply (I_P)	35	A
Voltage of DC power supply (V_{DC})	50	V
Peak voltage of pulsed power supply (V_P)	60	V
Pulse on time of pulsed power supply (t_{on})	20	μs
Pulse off time of pulsed power supply (t_{off})	20	μs
Flushing pressure	4, 6, 8, and 10	MPa
Rotational speed	100, 500, 1000, 1500, and 2000	rpm
Workpiece polarity	Positive	–

parameters were 8 MPa, 50 A, and 2000 rpm for dielectric flushing pressure, DC current and electrode rotational speed respectively. It is clear from the figure that with the increase in workpiece thickness, the MRR tends to decrease for both EDM and HEDAM. This is due to the ineffective flushing with increasing depths, which leads the machining debris to remain trapped at the bottom of the hole. This leftover debris in the machining gap leads to frequent electrode retractions and secondary discharges, which hampers the machining speed. However, HEDAM exhibited better performance in terms of MRR even at higher depths (30 mm) of drilling. The average machining time for drilling 30 mm depth in Inconel 718 using HEDAM is 3 min and 40 s, which is far less than conventional EDM. Additionally, HEDAM is more energy efficient compared to conventional EDM [11].

4.3 Mechanism of material removal and debris formation

The experiments were conducted for a small duration of 4 s to analyze the mechanism of material removal and the debris formation. The selected parameters were 50 A current from DC power supply, flushing pressure of 8 MPa and electrode rotation speed of 2000 rpm. Firstly, the tool electrode descends to reduce the machining gap between the electrode and the workpiece. As soon as the gap reaches a critical value, the dielectric fluid ionizes causing the occurrence of a HEDAM discharge. The formation of discharge arcs in the machining gap during HEDAM, causes the thermal energy density to elevate. This leads to the quick melting of workpiece material, leaving behind a crater on the workpiece surface and resulting in the formation of molten debris. In order to obtain stable operation, successful evacuation of debris from the machining zone is very essential [12].

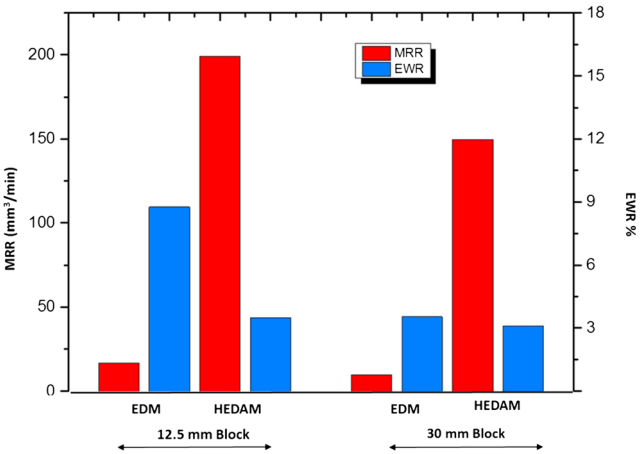

Fig. 5 Comparative study of EDM and HEDAM process for different thicknesses of the Inconel 718 workpiece

In any electrical arc machining process, formation of stationary arc is undesirable as it damages both the workpiece and electrode surfaces [13]. Therefore, to avoid stationary arc and facilitate relative motion between the workpiece and electrode, high-speed rotation (2000 rpm) of the tool electrode was employed. Moreover, the high pressure dielectric fluid instigates an intense hydrodynamic force which eventually breaks the arc plasma channel [10]. The combination of high-speed rotation and strong hydrodynamic force of dielectric fluid ultimately ruptures the plasma channel creating a shockwave which blows-off the molten debris from the machining zone in an eruptive manner. Fresh dielectric fluid rushes into the machining gap flushing out the remains and cooling the surface of the workpiece. Thus, the mechanism of material removal in HEDAM can be summarized by thermal melting due to striking arcs, followed by the ejection of molten debris due to the shockwave created by the explosion of plasma channel as shown in Fig. 6a.

Figure 6b–e shows the SEM images of the machined surface of Inconel 718 after HEDAM for a short duration of 4 s. To comprehend the importance of high pressure flushing in HEDAM, an experiment was conducted without dielectric flushing, the effect of which can be seen in Fig. 6b. It is evident from Fig. 6b that the molten debris get stagnated and resolidified in the absence of hydrodynamic force due to lack of high pressure flushing. However, owing to pressurized flushing in the subsequent experiment, the molten debris starts to flow as shown in Fig. 6c. It is also interesting to observe that the ejection of molten debris in an explosive fashion results in

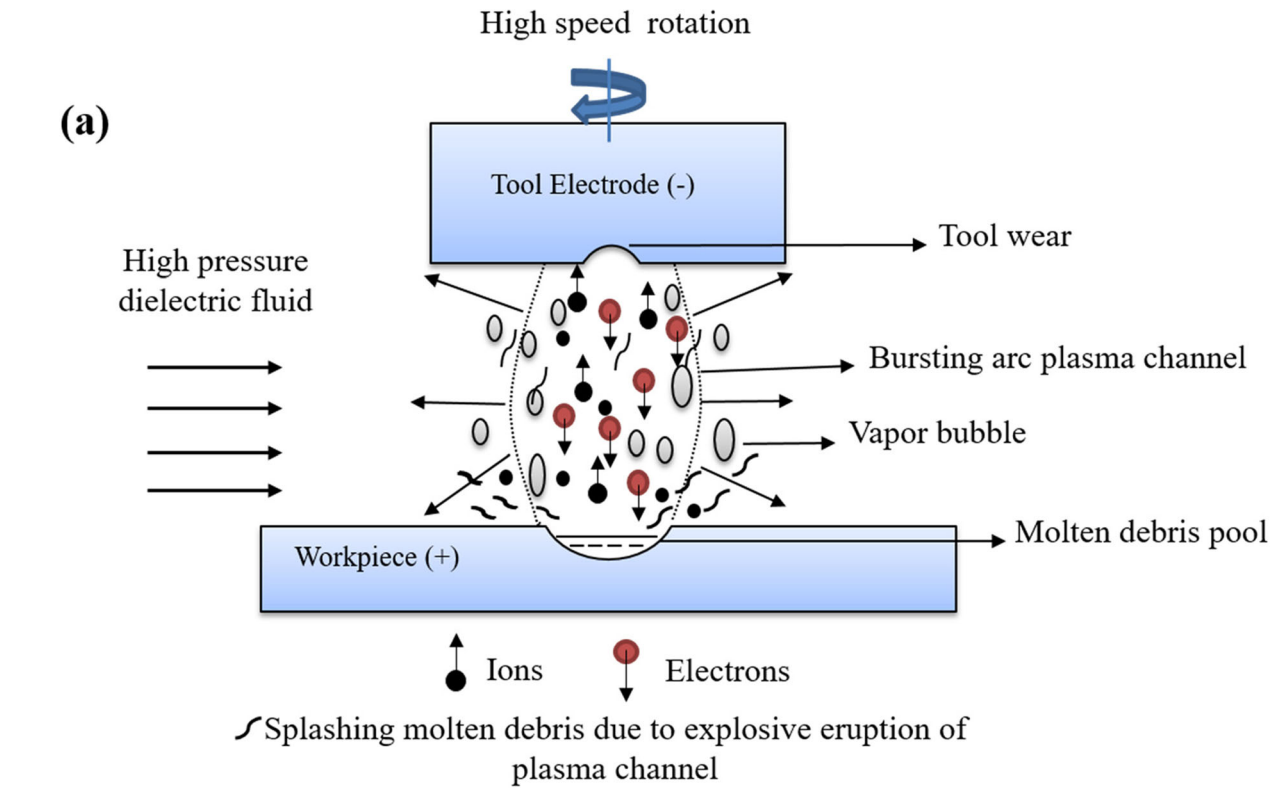
High speed rotation
(a)
Tool Electrode (-)
Tool wear
High pressure
dielectric fluid
Bursting arc plasma channel
Vapor bubble
Molten debris pool
Workpiece (+)
Ions
Electrons
Splashing molten debris due to explosive eruption of
plasma channel

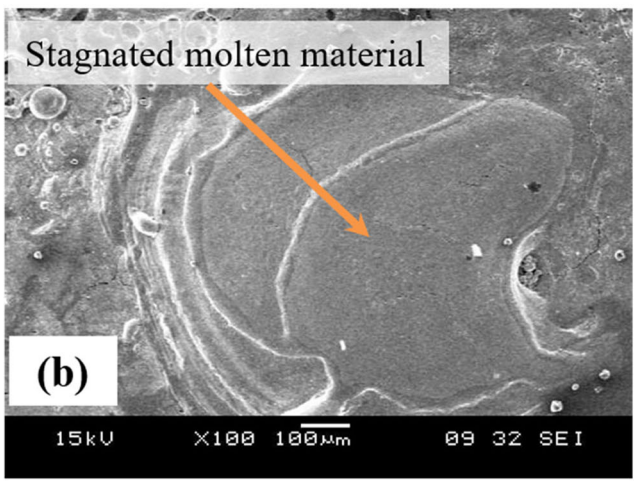
Stagnated molten material
(b)
15kV X100 100µm 09 32 SEI

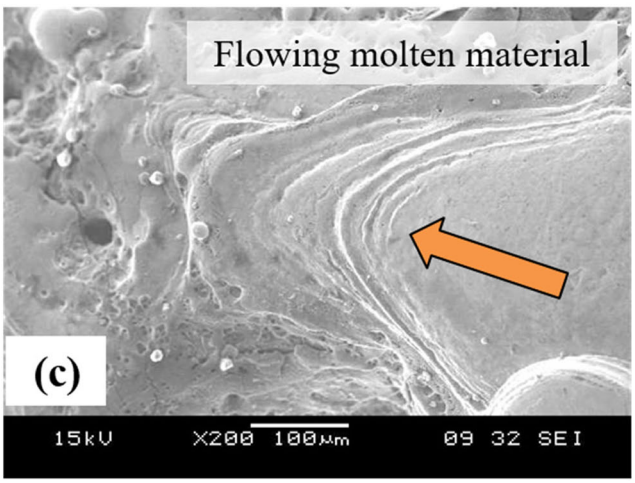
Flowing molten material
(c)
15kV X200 100µm 09 32 SEI

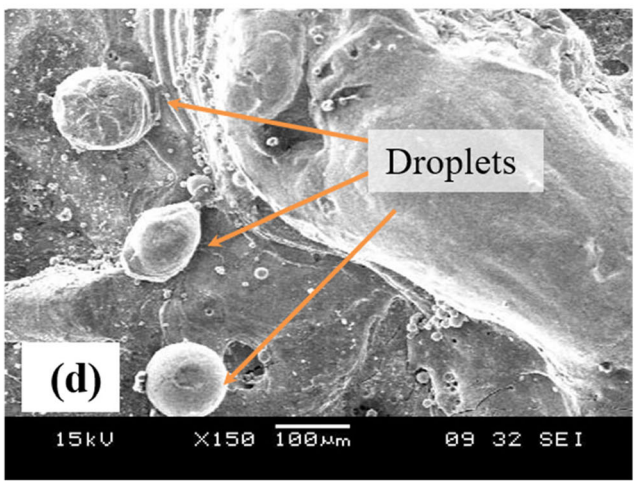
Droplets
(d)
15kV X150 100µm 09 32 SEI

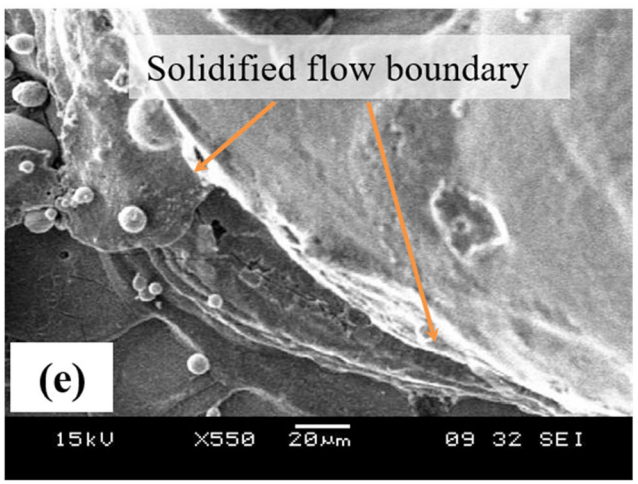
Solidified flow boundary
(e)
15kV X550 20µm 09 32 SEI

◀ **Fig. 6** **a** Schematic showing explosive eruption of arc plasma channel. **b** Stagnated molten debris. **c** Flowing molten debris. **d** Resolidified droplets. **e** Solidified crater boundary

the splashing of molten liquid which deposits on the workpiece as spherical droplets as depicted in Fig. 6d. The solidified flow boundary, where the molten debris flow has ended, can also be seen in Fig. 6e.

5 Results and discussion for HEDAM drilling

5.1 Effect of peak current on MRR and EWR

The effect of current on MRR and EWR for the HEDAM drilling of Inconel 718 is shown in Fig. 7. It can be observed that MRR increases with increasing current and a maximum MRR of 355 mm^3/min is achieved at 140 A. Similar trend was reported by Kuppan et al. [14] while deep hole EDM drilling of Inconel 718. The increase in MRR is attributed to the elevated thermal energy intensity with the increase of current in the machining gap.

High thermal energy results in higher melting rate during each cycle. Also, the larger size of the spark radius in HEDAM contributes to the increase of MRR [11]. On the other hand, there is a slight increase in the EWR with current during HEDAM process.

5.2 Effect of flushing pressure on MRR and EWR

During HEDAM drilling, the flushing pressure of the dielectric fluid plays a vital role on the machining performance. In early 1980s, Meshcheriakov proposed arc machining and found that the hydrodynamic pressure of the working fluid in the machining gap influences the physical features of the arc [15]. Figure 8 shows the effect of flushing pressure on the MRR and EWR for the HEDAM drilling of Inconel 718.

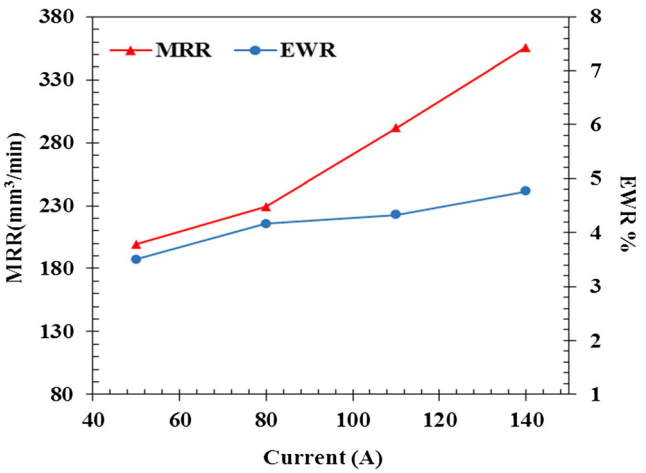

Fig. 7 Effect of current on MRR and EWR at 8 MPa and 2000 rpm

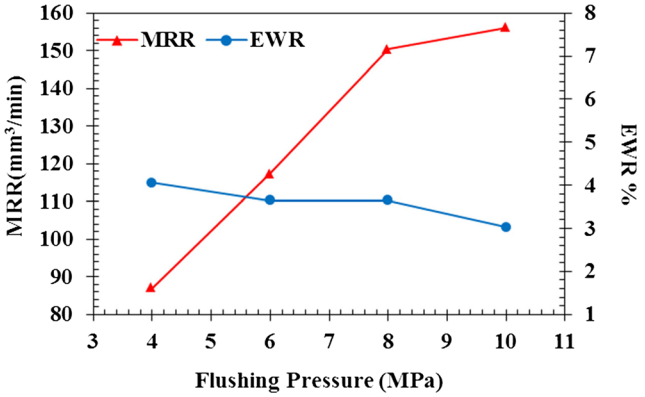

Fig. 8 Effect of flushing pressure on MRR and EWR at 50 A and 2000 rpm

The MRR shows an increasing trend with the increase in the flushing pressure due to the swift removal of molten debris from the machining gap. At low pressure (4 MPa), the dielectric fluid cannot effectively expel molten material from machining zone. This results in unstable machining with frequent electrode retractions. Hence, the machining operation gets increasingly interrupted resulting in low MRR. Thus, it is necessary to elevate the flushing pressure to improve the debris removal procedure.

With the increasing flushing pressure, EWR shows a decline after 4 MPa and the trend continues until the pressure value reaches 10 MPa. This is because at low flushing pressure of 4 MPa, the debris cannot be efficiently flushed out of the machining gap. As volumetric removal of workpiece decreases, EWR escalates. In addition, increasing the flushing pressure enhances the cooling effect of the tool electrode, thereby reducing the tool wear and EWR.

5.3 Effect of rotational speed on MRR and EWR

The effect of rotational speed on MRR and EWR during HEDAM drilling of Inconel 718 is shown in Fig. 9. MRR

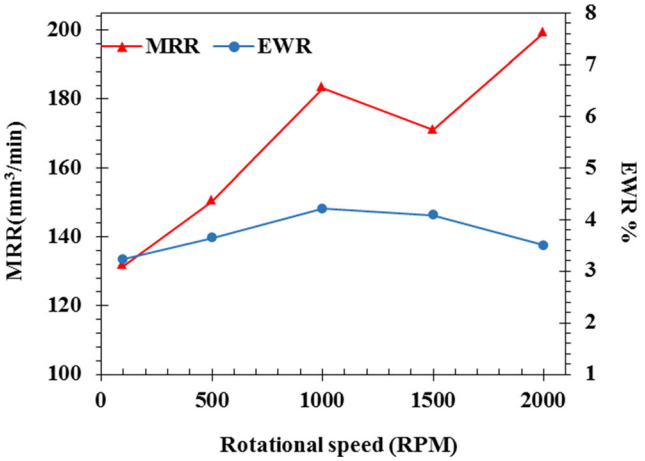

Fig. 9 Effect of rotational speed on MRR and EWR at 50 A and 8 MPa

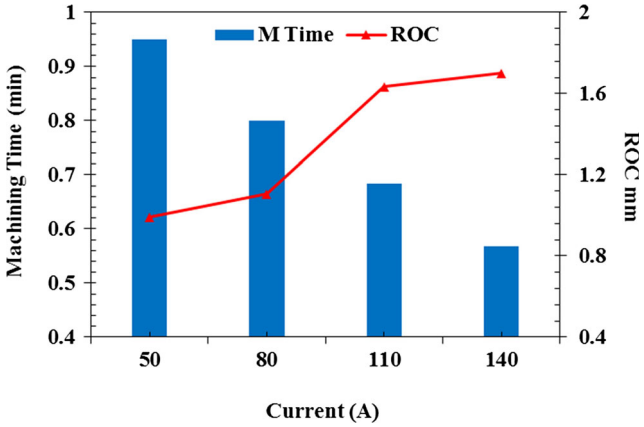

Fig. 10 Effect of current on machining time and ROC at 50 A, 8 Mpa, and 2000 rpm

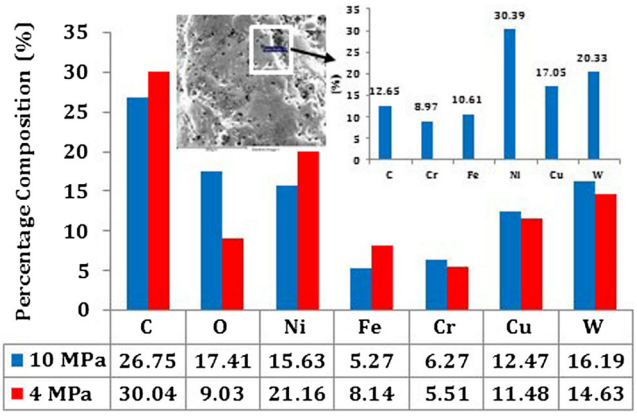

	C	O	Ni	Fe	Cr	Cu	W
10 MPa	26.75	17.41	15.63	5.27	6.27	12.47	16.19
4 MPa	30.04	9.03	21.16	8.14	5.51	11.48	14.63

Fig. 12 Percentage composition of the electrode tip after machining

shows a slightly increasing trend for the speed range of 100–2000 rpm. However, the evacuation of debris from the machining zone in HEDAM process is not the same as EDM. In the case of EDM, machined debris is in the form of small particles. With the increase in the rotational speed, the centrifugal force and the whirl facilitate the effective flushing of the fine debris from the machining gap. However, in the case of HEDAM, the machined debris is in the form of molten material due to the high discharge energy of arcs in the machining gap. The dense molten material has a tendency to settle down and is less readily flushed off by the low rotation speed of the tool due to inefficient arc breaking which causes the MRR to fall. Thus, it is necessary to increase the rotational speed to

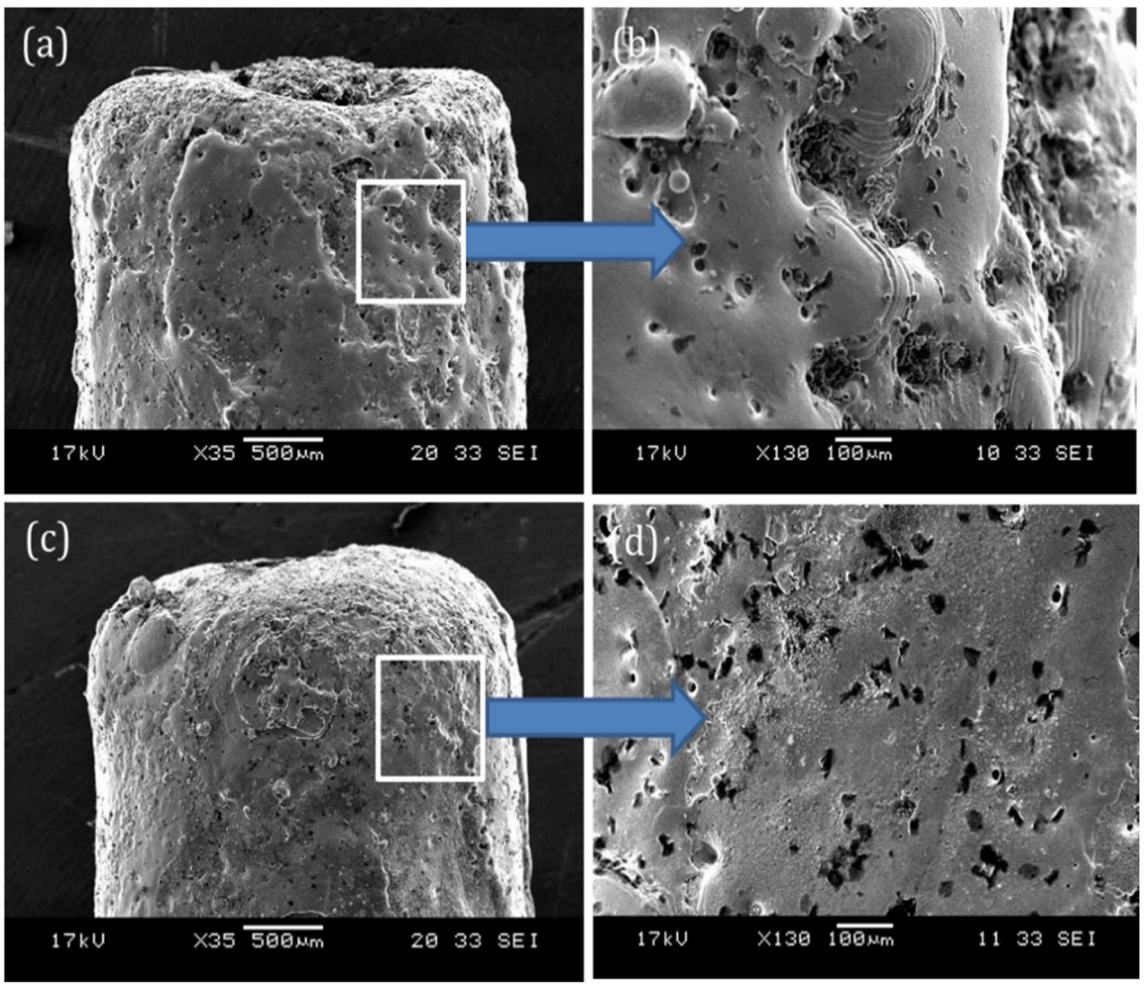

Fig. 11 SEM micrographs at (a) 4 MPa and (c) 10 MPa, and magnified view at (b) 4 MPa and (d) 10 MPa of the CuW electrode

facilitate the breakage of the plasma channel and to introduce fresh dielectric effectively in the machining gap. This new layer of dielectric provides an environment for better machining condition in the gap, which improves MRR.

However, it is also interesting to note that when the rotational speed of the electrode reaches 1500 rpm a sudden dip in MRR is observed. This is caused due to resonance of CuW electrode at that particular speed. As the rotational speed rises, the wobbling tendency of the free end of the electrode increases. Moreover, when it reaches the critical speed at which the resonance occurs, frequent electrode retractions take place due to repeated short-circuiting. This ineffective machining causes the reduction in MRR. The detailed calculation of critical resonance speed for CuW electrode is given in Appendix A. On the other hand, EWR does not show any significant trend with variation in rotational speed.

5.4 Effect of current on machining time and radial overcut

Figure 10 shows the machining time and radial overcut (ROC) for drilling holes in Inconel 718. At 50 A, it takes around 57 s to machine a through hole in a 12.5-mm thick block of Inconel 718. The time reduces to 34 s with a current value of 140 A from the DC power supply. However, in the case of EDM it takes much longer to drill a hole with the same depth. The ROC depicts an increasing trend with increase in current.

At the low current, the erosion of the workpiece is less, resulting in a low radial overcut. However, with the increasing current, the size of the plasma channel becomes bigger and creates deeper and larger crater on the workpiece. This accounts for the large ROC. Moreover, CuW provides high overcut due to the high spark dispersing effect, which explains the slightly higher overcut all across the board [16].

5.5 Analysis of the electrode after machining

Figure 11 shows the SEM micrographs of the CuW electrode tip after machining under the lowest (4 MPa) and the highest (10 MPa) flushing pressures. It can be seen that for 4 MPa pressure, the electrode suffers more damage when compared to 10 MPa. Also, there is more re-solidification at the lower flushing pressure due to inefficient flushing. The higher re-solidification at lower pressure is evident when the magnified images in Fig. 11(b), (d) are compared.

Figure 12 shows the percentage composition of the constituents present in the electrode tip after machining under the minimum and maximum flushing pressures. The EDX results confirm the migration of materials from the workpiece to the electrode tip during HEDAM. However, a higher percentage of the major constituents of Inconel 718 (Ni, Fe) were found for the flushing pressure of 4 MPa than for 10 MPa. This is due to relatively less efficient flushing at a low flushing pressure, which allows more workpiece debris re-solidification on the electrode tip.

This is also evident from the spot EDX performed on the resolidified layer (at 4 MPa) as shown in Fig. 12. Additionally, the deposition of carbon is higher for 4 MPa. The carbon element may result from the decomposition of fatty acid present in the water-based dielectric. Furthermore, it is observed that there is a significant difference in the amount of oxygen element between these two pressure settings. Oxygen is highly reduced from 17.41 to 9.03% for 10 MPa and 4 MPa respectively. Usually, the oxygen comes from the water-based dielectric used for the experiments. Due to the high temperature in the plasma channel, oxygen disassociates from the water in the dielectric. The free oxygen then oxidizes the tool material. The EDX spectrums of electrodes after HEDAM at 10 and 4 MPa are presented in Fig. 13.

5.6 Microstructural analysis

Figure 14 shows the microstructural images of the cross section near the machined surface and the base material. The purpose of conducting microstructural analysis is to compare the change of the grain structure/size in the heat-affected zone (HAZ) and the base material due to HEDAM. It is clear from the images that there is a significant difference in the microstructure in the HAZ compared to the base material. The grain size in the HAZ is observed to be much smaller than the bulk material. This is due to the quenching effect caused by high

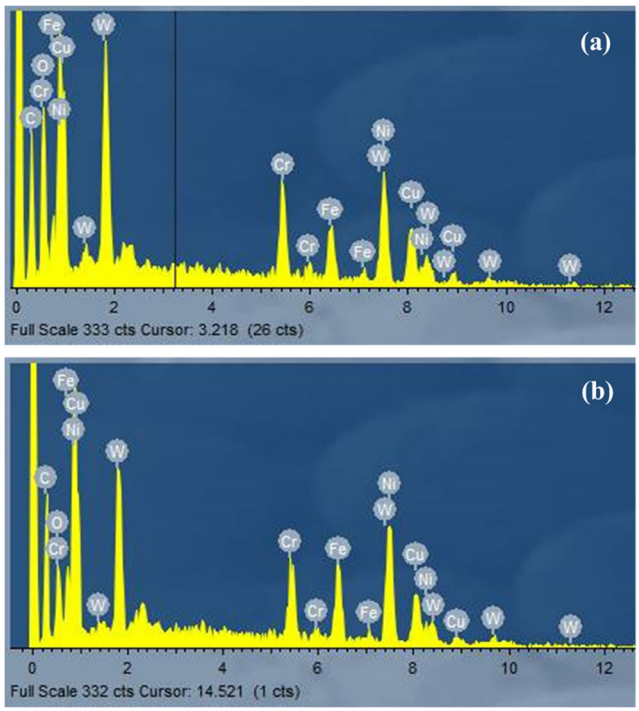

Fig. 13 EDX spectrums. **a** 10 MPa. **b** 4 MPa

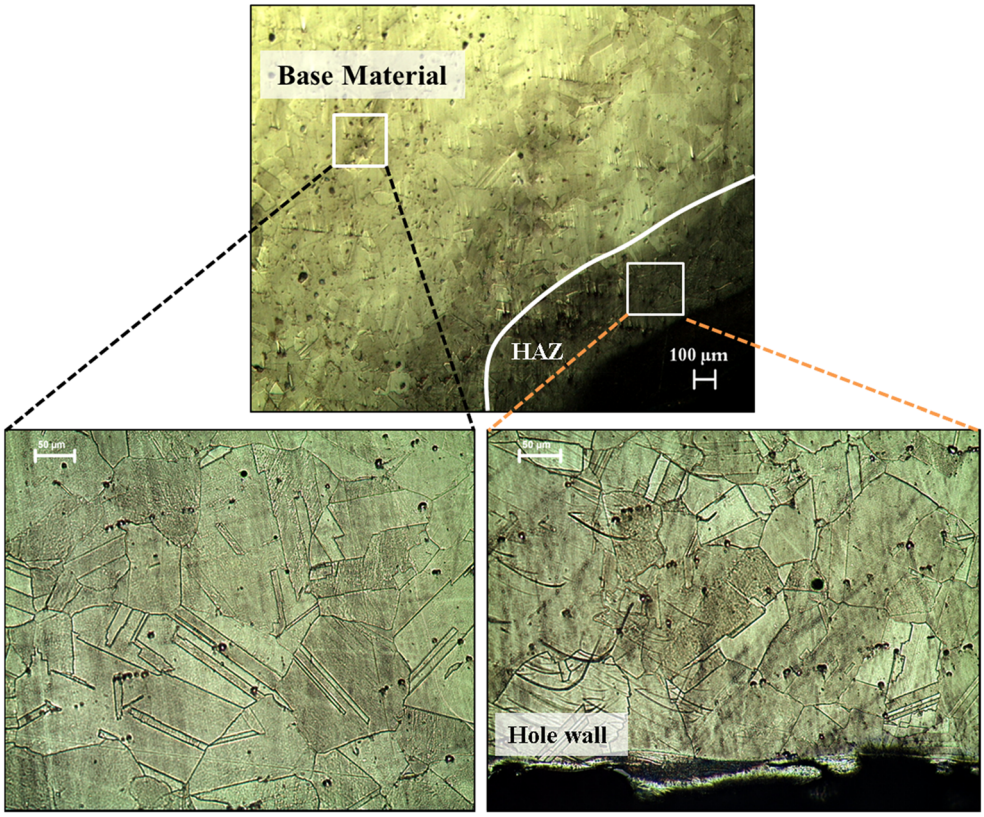

Fig. 14 Comparison of microstructure in the base material and heat-affected zone (HAZ)

temperature arcs followed by the immediate cooling of dielectric fluid in the machining gap.

Another possible reason for this change could be the low thermal conductivity of Inconel 718, which does not allow the quick dissipation of heat from the machining zone. This stagnated heat around the machining zone enhances the effect of quenching which results in a finer grain structure in the HAZ.

5.7 Microhardness analysis

Figure 15 shows the variation of microhardness at the cross section after HEDAM drilling at 50 A and 140 A. The test conditions and indentation marks at different current settings are shown in the figure as well. The trend of microhardness obtained at 50 A is similar to that at 140 A. Near the machined

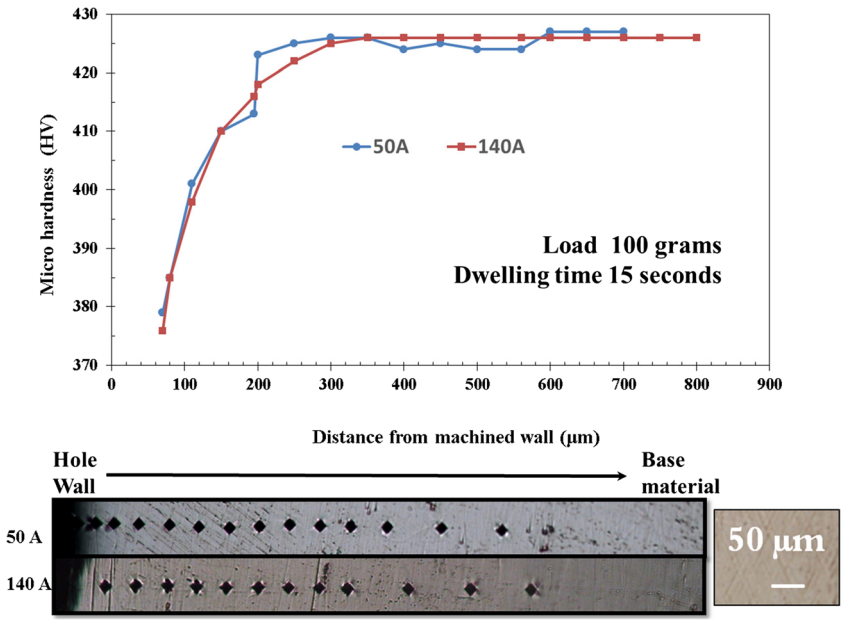

Fig. 15 Variation of microhardness from the machined wall after HEDAM drilling of Inconel 718 at 50 A and 140 A with 8 MPa and 2000 rpm

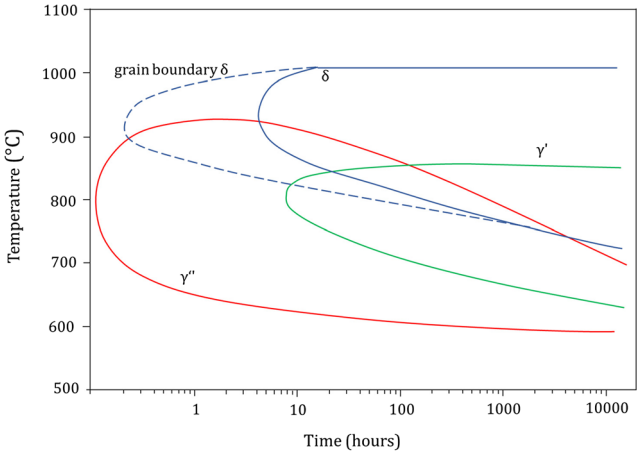

Fig. 16 Precipitation time temperature (PTT) diagram for Inconel 718 [17]

wall, the microhardness test shows a value of 375 HV, which gradually increases with the distance moved away from the machined zone. Eventually, at about 220 μm from the machined wall, the hardness reaches the bulk hardness of Inconel 718; 427 HV. This reveals that the bulk material is much harder than that at HAZ.

This variation of hardness is a direct consequence of the precipitation of various phases at different temperatures in Inconel 718. Ni and Cr in Inconel 718 crystallize as a γ phase (FCC). Niobium (Nb) is added to form hardening precipitates γ″ (centered tetragonal structure). Ti and Al are added to precipitate in the form of γ′ (simple cubic crystal). These precipitate phases (γ″ and γ′) are jointly responsible for the hardening strength of Inconel 718.

Due to increase in temperature near the machining zone during HEDAM, precipitation of δ phase is more prominent along the grain boundaries of the γ matrix. This δ phase is a stable phase with orthorhombic structure. This phenomenon of formation of δ precipitates is also evident from the precipitation time temperature (PTT) diagram for Inconel 718. A typical PTT diagram for Inconel 718 alloy is shown in Fig. 16.

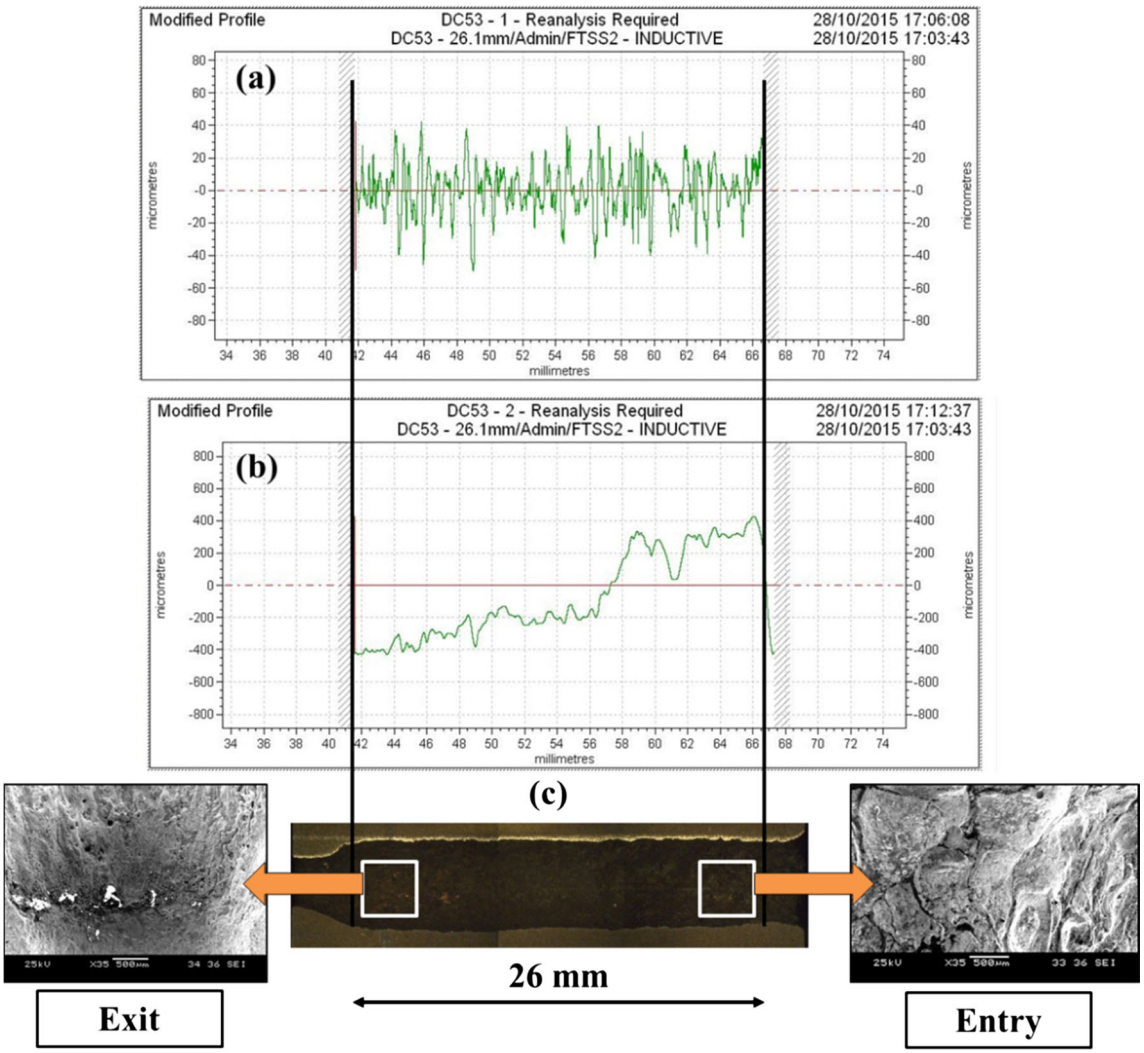

Fig. 17 Surface roughness and profile of HEDAM

Due to the reduction in the precipitation of γ'' and γ' hardening phases in the HAZ, the microhardness of the machined wall decreases after HEDAM. However, the heat does not seep deep into the bulk material. Hence, not much variation in microhardness is seen away from the machined wall.

5.8 Surface roughness and profile analysis

Figure 17 shows the surface roughness and profile analysis of the HEDAM drilled hole. The drilling depth was 30 mm in Inconel 718 workpiece with optimum settings of 50 A DC current, 8 MPa flushing pressure and 2000 rpm electrode rotational speed.

The hole after HEDAM drilling is sectioned using wire-EDM as shown in Fig. 17(c). Taylor Hobson profilometer was used to evaluate the roughness and the surface profile of the hole wall. The scanning was carried out at the middle section of the hole to avoid irregularities near the entry and exit sides due to stray sparking/arcing. The average surface roughness was found to be 10.11 μm.

The surface profile of the hole wall is shown in Fig. 17(b). It is clear from the figure that there is a gradual elevation in profile towards the entry side of the hole wall. This is attributed to the deposition/re-solidification of the molten debris while flowing through the annulus (machining gap). This is also evident from the SEM micrograph shown in Fig. 17(c). In addition, as the electrode approaches the exit/bottom of the hole, the tendency of secondary discharges occurring at the peripheral surface of electrode increases. Due to this, deeper craters are formed at the sides, which shows up as the depressions in the surface profile near the exit of the hole wall.

6 Conclusion

In this paper, a study on the design and development of HEDAM was presented. The variation of MRR and EWR with different operating parameters, material removal phenomenon, microstructural analysis, surface roughness analysis and microhardness have also been investigated in details. Based on these studies, the following conclusions can be drawn:

- HEDAM provides a high-speed non-contact way of drilling difficult-to-cut materials like Inconel 718.
- In HEDAM, the mechanism of material removal is thermal melting followed by ejection of the molten debris by the shockwave generated due to explosive eruption of arc plasma channel. The eruption is caused owing to the combination of high-speed rotation of the electrode which elongates the plasma channel followed by breaking off due to high pressure dielectric fluid.
- The MRR for HEDAM showed an increasing trend with increasing current, flushing pressure and rotation speed of the electrode. A maximum MRR of 355 mm^3/min was achieved at 140 A, 8 MPa, and 2000 rpm.
- Increase in the flushing pressure resulted in the quick removal of the molten debris and proper deionization of the plasma channel leading to an increased MRR. EWR showed a decreasing trend due to a better cooling effect of the electrode at high flushing pressure.
- There is migration and re-solidification of the material from the workpiece to the electrode tip. Higher pressure flushing reduces the amount of re-solidification.
- Microstructural analysis showed finer grain structure in the HAZ. Moreover, the microhardness analysis of the HAZ revealed it to be softer than the bulk material.
- The average surface roughness of the HEDAM drilled surface is 10.11 μm.
- The study clearly establishes the feasibility of using a HEDAM process for efficient machining of difficult-to-cut materials like Inconel 718.

Acknowledgements The authors would like to thank Dr. S. Panda and Mr. J. Adhikari for their contributions.

Funding information This work was funded by A*Star (Grant No. R265-000-534-305) and Singapore Institute of Manufacturing Technology (SIMTech) (Grant No. R265-000-518-504).

Appendix A. Calculation of critical rotational speed for CuW pipe electrode

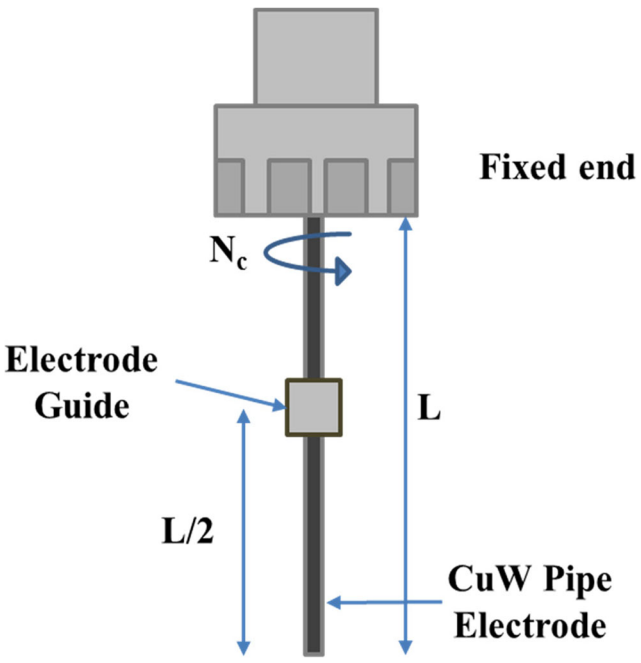

Fig. 18 Schematic diagram of the CuW electrode-guide

Dimensions and properties of CUW electrode
Length of the electrode (L) = 175 mm
Outer diameter of the electrode (D) = 3 mm
Inner diameter of the electrode (d) = 0.8 mm
Modulus of elasticity (E) = 620 MPa
Density (ρ) = 1450 kg/m^2

According to Abbas et al. [8], the critical speed of rotation for the case shown in Fig. 18 is given by:

$$\omega = \frac{\beta^2}{L^2}\sqrt{\frac{EI}{\rho A}} \quad (1)$$

where β = Eigen value for beams with clamped-simple-free support
= 3.1 for the case shown in Fig. 18 [18].
I = area moment of inertia
Substituting the values in Eq. (1):

$$\omega = \frac{3.1^2}{0.175^2}\sqrt{\frac{620 \times 10^6 \times 3.95 \times 10^{-12}}{1450 \times 6.56 \times 10^{-6}}}$$
$$\omega = 159.09 \text{ rad}/s$$

Now, frequency $(f) = \frac{\omega}{2\pi}$ = 25.33 Hz
Critical speed of rotation can be found as $N_c = f \times 60$ = 1520 rpm

Hence, the critical speed at which the CuW electrode experiences resonance is around 1520 rpm.

References

1. Sharman A, Dewes RC, Aspinwall DK (2001) Tool life when high speed ball nose end milling Inconel 718. J Mater Process Technol 118(1):29–35
2. Ezugwu EO, Wang ZM, Machado AR (1999) The machinability of nickel-based alloys: a review. J Mater Process Technol 86(1):1–16
3. Rahman M, Seah WKH, Teo TT (1997) The machinability of Inconel 718. J Mater Process Technol 63(1–3):199–204
4. Li L, He N, Wang M, Wang ZG (2002) High speed cutting of Inconel 718 with coated carbide and ceramic inserts. J Mater Process Technol 129(1):127–130
5. Guo YB, Li W, Jawahir IS (2009) Surface integrity characterization and prediction in machining of hardened and difficult-to-machine alloys: a state-of-art research review and analysis. Mach Sci Technol 13(4):437–470
6. Li ZY, Wei XT, Guo YB, Sealy MP (2015) State-of-art, challenges, and outlook on manufacturing of cooling holes for turbine blades. Mach Sci Technol 19(3):361–399
7. Kunieda M, Lauwers B, Rajurkar KP, Schumacher BM (2005) Advancing EDM through fundamental insight into the process. CIRP Ann Manuf Technol 54(2):64–87
8. Abbas NM, Solomon DG, Bahari MF (2007) A review on current research trends in electrical discharge machining (EDM). Int J Mach Tools Manuf 47(7–8):1214–1228
9. Kiyak M, Cakır O (2007) Examination of machining parameters on surface roughness in EDM of tool steel. J Mater Process Technol 191(1–3):141–144
10. Zhao W, Gu L, Xu H, Li L, Xiang X (2013) A novel high efficiency electrical erosion process–blasting erosion arc machining. Procedia Cirp 6:621–625
11. Ahmed A, Fardin A, Tanjilul M, Wong YS, Rahman M, Kumar AS (2018) A comparative study on the modelling of EDM and hybrid electrical discharge and arc machining considering latent heat and temperature-dependent properties of Inconel 718. Int J Adv Manuf Technol 94(5–8):2729–2737
12. Tanjilul M, Ahmed A, Kumar AS, Rahman M (2018) A study on EDM debris particle size and flushing mechanism for efficient debris removal in EDM-drilling of Inconel 718. J Mater Process Technol 255:263–274
13. Xu H, Gu L, Chen J, Hu J, Zhao W (2015) Machining characteristics of nickel-based alloy with positive polarity blasting erosion arc machining. Int J Adv Manuf Technol 79(5–8):937–947
14. Kuppan P, Rajadurai A, Narayanan S (2008) Influence of EDM process parameters in deep hole drilling of Inconel 718. Int J Adv Manuf Technol 38(1–2):74–84
15. Meshcheriakov G, Nosulenko V, Meshcheriakov N, Bokov V (1998) Physical and technological control of arc dimensional machining. CIRP Ann Manuf Technol 37(1):209–212
16. Singh S, Maheshwari S, Pandey PC (2004) Some investigations into the electric discharge machining of hardened tool steel using different electrode materials. J Mater Process Technol 149(1–3): 272–277
17. Thomas A, El-Wahabi M, Cabrera JM, Prado JM (2006) High temperature deformation of Inconel 718. J Mater Process Technol 177(1–3):469–472
18. Gorman DJ (1974) Free lateral vibration analysis of double-span uniform beams. Int J Mech Sci 16(6):345–351